



Providing Choice & Value
Generic CT and MRI Contrast Agents



**FRESENIUS
KABI**

CONTACT REP

AJNR



Does CISS MRI Reliably Depict the Endolymphatic Duct in Children with and without Vestibular Aqueduct Enlargement?

Olutayo I. Olubiyi, Nicholas Thompson, Thad Benefield,
Kassie L. McCullagh and Benjamin Y. Huang

This information is current as
of July 21, 2025.

AJNR Am J Neuroradiol published online 29 February 2024
<http://www.ajnr.org/content/early/2024/02/29/ajnr.A8158>

Does CISS MRI Reliably Depict the Endolymphatic Duct in Children with and without Vestibular Aqueduct Enlargement?

 Olutayo I. Olubiyi,  Nicholas Thompson,  Thad Benefield, Kassie L. McCullagh, and  Benjamin Y. Huang

ABSTRACT

BACKGROUND AND PURPOSE: High-resolution CT is the mainstay for diagnosing an enlarged vestibular aqueduct (EVA), but MR imaging may be an appealing alternative, given its lack of ionizing radiation exposure. The purpose of this study was to determine how reliably MR imaging demonstrates the endolymphatic duct and endolymphatic duct enlargement in hearing-impaired children.

MATERIALS AND METHODS: We performed a retrospective review of temporal bone high-resolution CT and MR imaging of hearing-impaired children evaluated between 2017 and 2020. Vestibular aqueduct diameter was measured on high-resolution CT. The vestibular aqueducts were categorized as being enlarged (EVA+) or nonenlarged (EVA−) using the Cincinnati criteria. The endolymphatic ducts were assessed on axial high-resolution CISS MR imaging. We categorized endolymphatic duct visibility into the following: type 1 (not visible), type 2 (faintly visible), and type 3 (easily visible). Mixed-effect logistic regression was used to identify associations between endolymphatic duct visibility and EVA. Interreader agreement for the endolymphatic duct among 3 independent readers was assessed using the Fleiss κ statistic.

RESULTS: In 196 ears from 98 children, endolymphatic duct visibility on MR imaging was type 1 in 74.0%, type 2 in 14.8%, and type 3 in 11.2%; 20.4% of ears were EVA+ on high-resolution CT. There was a significant association between EVA+ status and endolymphatic duct visibility ($P < .01$). Endolymphatic duct visibility was type 1 in 87.1%, type 2 in 12.8%, and type 3 in 0% of EVA− ears and type 1 in 22.5%, type 2 in 22.5%, and type 3 in 55.0% of EVA+ ears. The predicted probability of a type 3 endolymphatic duct being EVA+ was 0.997. There was almost perfect agreement among the 3 readers for distinguishing type 3 from type 1 or 2 endolymphatic ducts.

CONCLUSIONS: CISS MR imaging substantially underdiagnoses EVA; however, when a type 3 endolymphatic duct is evident, there is a >99% likelihood of an EVA.

ABBREVIATIONS: ELD = endolymphatic duct; ELS = endolymphatic sac; EVA = enlarged vestibular aqueduct; HRCT = high-resolution CT; IAC = internal auditory canal; SNHL = sensorineural hearing loss; VA = vestibular aqueduct

Imaging constitutes an important part of the evaluation of children with hearing loss, with the primary imaging modalities being high-resolution CT (HRCT) of the temporal bone and focused MR imaging evaluation of the inner ear and internal auditory canals (IACs).¹ Enlargement of the vestibular aqueduct (VA) is among the most common abnormal imaging findings identified in patients with congenital deafness, and it is implicated in approximately 12% of children with congenital sensorineural hearing loss (SNHL).^{2,3}

The diagnosis of an enlarged vestibular aqueduct (EVA) is important to explain audiologic findings, to allow appropriate genetic testing and counseling, to advise patients of the risk of progressive hearing loss from participation in contact sports, to predict the presence of other labyrinthine anomalies on imaging, and to determine potential risks of cochlear implantation such as a perilymphatic gusher.⁴ Traditionally, HRCT has been the mainstay for imaging evaluation of patients with hearing loss and for diagnosing EVA. While an MR imaging correlate to EVA, the enlarged endolymphatic duct syndrome, has been described,⁵ MR imaging has been largely used as an adjunct tool in evaluating these patients.^{6–8} However, MR imaging has several potentially compelling advantages over CT, including its lack of ionizing radiation exposure as well as its improved ability to demonstrate perilymph in the inner ear and structures not directly visualized on HRCT such as the cochleovestibular nerve.⁹ Being able to perform a complete imaging assessment of the inner ear with a single

Received May 24, 2023; accepted after revision December 23.

From the Division of Neuroradiology, Department of Radiology (O.I.O.), Department of Otolaryngology (N.T.), and Department of Radiology (T.B., K.L.M., B.Y.H.), University of North Carolina School of Medicine, Chapel Hill, North Carolina; Commonwealth Radiology PC (O.I.O.), Richmond, Virginia; and University of North Carolina Hospitals (K.L.M.), Chapel Hill, North Carolina.

Please address correspondence to Olutayo I. Olubiyi, MB, ChB, MPH, Commonwealth Radiology PC, Radiology, St. Mary's Hospital, 5801 Brems Rd, Richmond, Richmond, VA 23226; e-mail: oio061@mail.harvard.edu

<http://dx.doi.org/10.3174/ajnr.A8158>

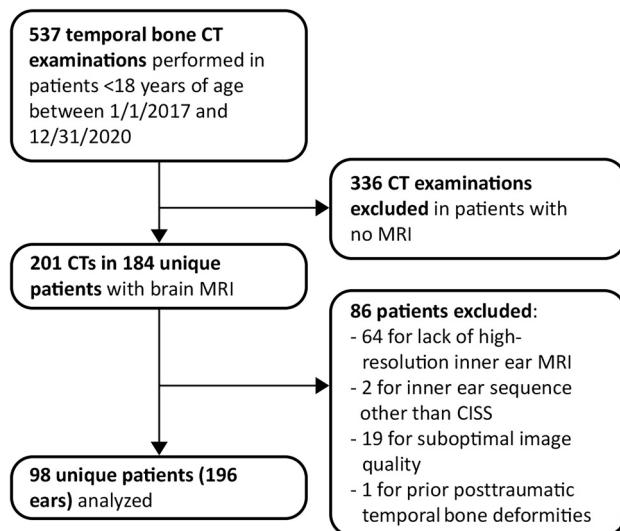


FIG 1. Flow chart summarizing identification, selection, and exclusion of subjects from this study.

test while avoiding radiation exposure in children with SNHL or suspected EVA would be a highly appealing proposition.

To date, several studies have investigated the utility of MR imaging compared with HRCT for diagnosing EVA;^{4,10-13} however, there is relatively sparse data¹³ on how reliably MR imaging is able to depict certain endolymph-containing structures, namely the endolymphatic duct (ELD) and the endolymphatic sac (ELS). The purpose of this study was to establish the following: 1) how often the ELD is visualized on routine high-resolution 3D fluid-sensitive MR imaging of the temporal bones, and 2) how reliably MR imaging can detect VA enlargement in children referred for imaging of hearing loss.

MATERIALS AND METHODS

This retrospective study was approved by our center's institutional review board (University of North Carolina) and approved with a waiver of the requirement for informed consent. Patients younger than 18 years of age who had a temporal bone HRCT on our PACS between January 2017 and December 2020 were initially identified. These patients were screened to identify those who also had a brain MR imaging that included high-resolution 3D fluid-sensitive sequences tailored to assess the inner ear structures. Patients were excluded if there was no MR imaging available for viewing on our PACS, if the MR imaging did not include high-resolution inner ear images, if either the HRCT or MR imaging studies were deemed suboptimal for evaluation due to excessive artifacts, or if there were posttraumatic deformities of the otic capsule. Because our routine temporal bone MR imaging protocol during the study period overwhelmingly used a CISS sequence for assessment of the inner ears, examinations that used sequences other than CISS were also excluded from our analysis to avoid potential heterogeneity related to use of multiple different pulse sequences. The algorithm used to identify subjects for the study is summarized in Fig 1.

A clinical chart review of each subject's electronic medical record was performed by a neurotology fellow, who recorded

patient demographic and clinical information including available audiometric data for each ear. The HRCT and MR images were initially reviewed by a first-year neuroradiology fellow who was blinded to the clinical data. All the scans and imaging data were subsequently overread by a senior attending neuroradiologist with >15 years of experience who was also blinded to the clinical data. Any discrepancies between the reviewers' interpretations were reconciled at a consensus review session. For the initial MR imaging review performed by the fellow and the senior attending physician, the readers were not blinded to the CT findings.

All temporal bone CT images were acquired axially and reconstructed at a 0.6-mm section thickness. To account for variations in patient head positioning, we reconstructed reformatted images of each temporal bone in the plane parallel to that of the ipsilateral horizontal semicircular canal (termed the "true axial plane") using the built-in Volume Viewing tool on our PACS. A second Pöschl view reconstruction was created along an approximately 45° oblique plane, parallel to the ipsilateral superior semicircular canal. The final VA evaluation was performed on magnified views of these reconstructed image sets in a standard bone window (width = 3900, level = 150). VA diameter in each ear was measured at the midpoint and operculum in the true axial plane according to the method described by Boston et al¹⁴ and at the midpoint in the 45° oblique Pöschl plane, similar to the technique described by Juliano et al.¹⁵ Each VA was then categorized as being either enlarged (EVA+) or normal (EVA-) based on the criteria proposed by Boston et al (the Cincinnati criteria), which considers the VA to be enlarged if its midpoint width in the axial plane is ≥ 1.0 mm or its operculum width is ≥ 2.0 mm.¹⁴

MR imaging examinations included 60 scans (61.2%) performed on a 3T system; and 38 scans (38.8%), on a 1.5T system. All MR images included high-resolution CISS sequences of the temporal bones. The high-resolution sequences featured isotropic or near-isotropic voxel widths ranging from 0.5 to 0.8 mm, 70.4% of which were 0.5 mm, 5.1% were 0.6 mm, and 23.4% were 0.7 mm. The transverse FOV for the CISS images was set to include both temporal bones in a single acquisition and ranged from 109 to 187 mm, with 90.0% being between 135 and 150 mm.

For each ear, the CISS images were subjectively evaluated for the visibility of the ELD, which was categorized into 1 of 3 types: type 1, the ELD not visible; type 2, the ELD faintly visible but indistinct and not subjectively enlarged; and type 3, the ELD distinct and easily visible or subjectively enlarged (Fig 2). Subjective enlargement was determined by the apparent width of the ELD clearly being greater than that of the ipsilateral lateral semicircular duct. Additional examples of type 2 and 3 ELD visibility are demonstrated in Figs 3 and 4 respectively. Because the ELD was not visible or is indistinct in most of our cases, precluding reliable measurements on MR imaging, we elected not to routinely measure ELD width, except in cases in which we thought the ELD could be reliably measured on our PACS, in which cases the axial midpoint diameter of the ELD was measured. When extraosseous ELSs were evident, the greatest orthogonal dimensions of the extraosseous portion of the ELS were measured in the axial plane.

To determine whether MR imaging visibility was associated with VA enlargement, we implemented mixed-effects logistic

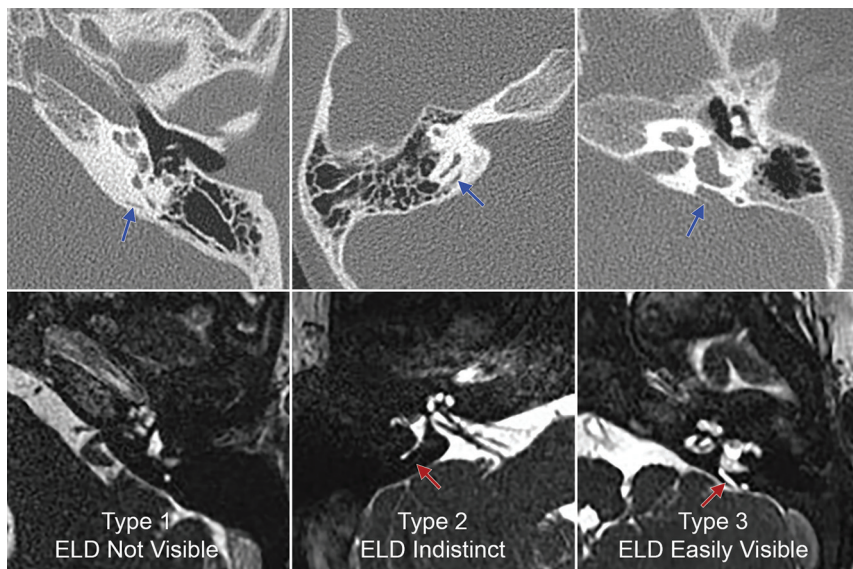


FIG 2. Examples of the 3 types of ELD visibility observed on MR imaging. *Upper row*, Representative axial-view non-contrast-enhanced temporal bone CT images of 3 different ears from different patients. *Lower row*, Axial temporal bone CISS MR images corresponding to the same ears as the CT images directly above demonstrate type 1 (lower left image), type 2 (lower middle image), and type 3 ELDs (lower right image). *Blue arrows* in the upper row indicate the vestibular aqueducts; *red arrows* in the lower row indicate the visible ELDs.

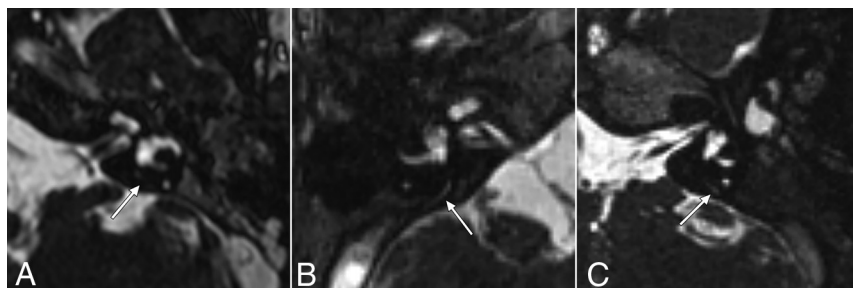


FIG 3. CISS MR images demonstrating additional examples of type 2 (faintly visible) ELDs (arrows) in 3 different patients: A, A 4-year-old girl with mild SNHL in the left ear. This patient demonstrated EVA on CT. B, A 1-year-old boy with profound SNHL in the right ear. This patient did not have VA enlargement on CT. C, An 8-year-old girl with profound SNHL in the left ear. This patient did not have VA enlargement on CT.

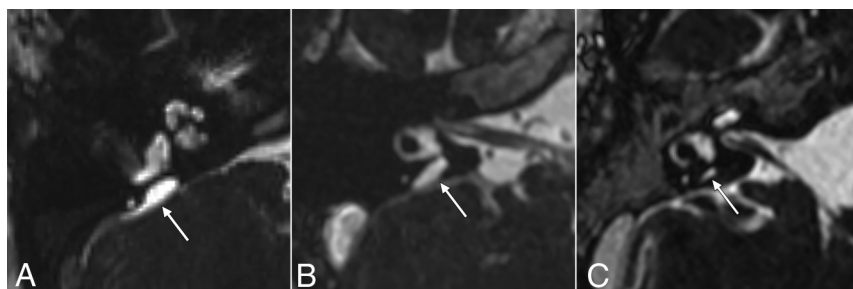


FIG 4. CISS MR images demonstrating additional examples of type 3 (easily visible) ELDs (arrows) in 3 different patients. A, A 7-month-old girl with severe SNHL in the right ear. B, A 6-year-old boy with severe SNHL in the right ear. C, A 4-year-old girl with mild SNHL in the left ear. All patients in these images demonstrated EVA on CT.

regressions with a logit link. In addition, to evaluate whether mean VA widths differ by MR imaging visibility, we implemented mixed-effects regressions, with separate models performed for

each VA measurement. For both sets of models, we included a random R-side compound-symmetric covariance term to account for correlations arising within patients since measurements were collected from both ears. Ear side and MR imaging scanner field strength were included as control variables, as well as the main independent variable, MR imaging visibility. A P value $< .05$ for the type 3 test for the effect of MR imaging visibility was considered evidence of an association or mean difference. When an association or mean difference was found, we computed predicted probabilities of enlargement or predicted mean VA widths for each MR imaging visibility category and 95% confidence intervals using observed margins of covariates. We also computed pair-wise tests of predicted probability or mean differences with P values adjusted using the Tukey method to preserve type 1 error. The initial consensus assessments by the neuroradiology fellow and senior neuroradiologist were used as the criterion standard for these analyses.

Because the fellow and senior attending physician performing the initial imaging review were not blinded to the CT findings, we further assessed interrater agreement in the MR imaging evaluation of ELD visibility by having the MR imaging examinations read separately by 2 additional readers, including a junior attending neuroradiologist with nearly 2 years of experience and the neurotologist who had initially gathered the clinical data and had since joined the faculty. The image review by the neurotologist was performed at least 1 year after the clinical data were collected, and both readers were blinded to the clinical data and CT examinations at the time of MR imaging review. Interreader agreement among the 3 readers (reader 1 = fellow and senior neuroradiologist; reader 2 = junior neuroradiologist; reader 3 = neurotologist) was assessed using the Fleiss κ statistic, including separate statistics by laterality because observations are not independent. The κ statistics, along with a large-sample confidence interval derived using the Δ method, were calculated for the 3 readers for the original 3-category outcome (type 1, type 2, or type 3 visibility)

and for a dichotomized outcome of no or faint MR imaging visibility (type 1 or type 2 MR imaging visibility) versus easy MR imaging visibility (type 3 MR imaging visibility). We also repeated the agreement analysis for pair-wise combinations of readers (reader 1 versus reader 2, reader 1 versus reader 3, and reader 2 versus reader 3).

RESULTS

A total of 537 temporal bone HRCT studies were identified on our PACS and subsequently screened for potential inclusion. For 201/537 HRCT studies, a brain MR imaging was also available for review. Fourteen patients were noted to have undergone multiple HRCT examinations (ranging from 2 to 4), ultimately yielding 184 unique patients with both HRCT and MR imaging for additional screening. Eighty-four patients were eventually excluded due to the MR imaging not including high-resolution inner ear sequences ($n = 64$); the HRCT or MR imaging being technically suboptimal due to significant motion, susceptibility, or other artifacts ($n = 19$); or the presence of significant posttraumatic or

postsurgical deformities of the temporal bones ($n = 1$). Two additional patients were excluded because their IAC MR imaging used a sequence other than CISS for inner ear characterization: T2-weighted, sampling perfection with application-optimized contrast by using different flip angle evolution (T2-SPACE sequence; Siemens) in 1 case and FIESTA in the other. A total of 98 patients and 196 ears were included in the final analysis (Fig 1). For patients with multiple HRCT or MR imaging scans available, the first of each scan type was used for imaging review unless it was deemed technically inadequate or if the initial MR imaging did not include high-resolution images through the inner ears; in the latter situation, the first MR imaging examination including high-resolution images was used.

The mean patient age at the time of HRCT was 6.2 (SD, 4.7) years. Fifty-three subjects (54.1%) were females. The median interval between HRCT and MR imaging was 62 days (interquartile range, 581.8 days). One child did not have audiometric data available for review. Of the remaining 97 children, 66 had bilateral hearing loss and 31 had unilateral hearing loss (Table 1). Of the 194 ears for which audiometry was available, 31 demonstrated normal hearing; 140, SNHL; 18, conductive hearing loss; and 5, mixed hearing loss (Table 2). Of note, the 2 ears in the child for whom audiometric data were unavailable both demonstrated VA enlargement on HRCT.

In 145/196 (74.0%) of the evaluated ears, the high-resolution temporal bone MR imaging sequence failed to demonstrate the ELD (type 1 visualization). In the remaining ears, the ELD was faintly visible (type 2 visualization) in 29/196 (14.8%) and was easily visible (type 3 visualization) in 22/196 (11.2%). Other inner ear and IAC imaging abnormalities were demonstrated in 23.4% of all ears, including dysmorphic cochlear and vestibular structures, the most common of which was an incomplete partition spectrum anomaly, observed in 8.1% of the evaluated ears.

On HRCT, midpoint VA widths measured in the axial plane ranged from 0 to 3.7 mm (median, 0.7 mm; mean, 0.84 [SD, 0.610] mm), while opercular widths ranged from 0 to 5.9 mm (median, 1.0; mean, 1.23 [SD, 0.92] mm). Midpoint VA widths measured in the Pöschl plane ranged from 0 to 3.8 mm (median, 0.6 mm; mean, 0.78 [SD, 0.54] mm).

A summary of rates of ELD visibility on MR imaging based on EVA status is presented in Table 3. Based on HRCT imaging, 40/196 ears (20.4%) in 25 children met the criteria for being EVA+ according to the Cincinnati criteria. There was a significant association between the presence of EVA on HRCT and ELD visibility on MR imaging ($<.001$). In the EVA- ears, ELD visibility on MR imaging was type 1 in 87.2%, type 2 in 12.8%, and type 3 in 0%. In EVA+ ears, ELD visibility was type 1 in 22.5%, type 2 in 22.5%, and type 3 in 55.0% (Table 3).

Table 1: Baseline demographic, audiometric, and imaging data

Patient-Level Characteristics	Overall ($n = 98$ Patients)
Demographic	
Age (mean) (SD) (yr)	6.2 (4.7)
Female sex (No.) (%)	53 (54.1)
Hearing loss laterality (No.) (%)	
Bilateral	66 (67.3)
Unilateral	31 (31.6)
Data not available	1 (1.0)
MR imaging field strength (No.) (%)	
1.5T (%)	38 (38.8)
3T (%)	60 (61.2)

Table 2: Baseline demographic, audiometric, and imaging data

Characteristics by Evaluated Ears	Overall ($n = 196$ Ears)
Type of hearing loss (No.) (%)	
Normal	31 (15.8)
Sensorineural	140 (71.4)
Conductive	18 (9.2)
Mixed	5 (2.5)
Audiometry data not available	2 (1)
Severity of hearing loss (No.) (%)	
Normal	31 (15.8)
Mild	15 (7.7)
Moderate	23 (11.7)
Severe	42 (21.4)
Profound	83 (42.3)
Audiometry data not available	2 (1)
ELD visualization (No.) (%)	
Type 1	145 (74.0)
Type 2	29 (14.8)
Type 3	22 (11.2)

Table 3: ELD visibility on high-resolution MR imaging based on EVA status

VA Status on CT ^a	Type of ELD Visualization on MR Imaging			Totals (Column %)
	Type 1, Not Visualized No. (Row %)	Type 2, Faintly Visualized No. (Row %)	Type 3, Easily Visualized No. (Row %)	
EVA –	136 (87.2)	20 (12.8)	0 (0)	156 (79.6)
EVA +	9 (22.5)	9 (22.5)	22 (55.0)	40 (20.4)
Totals (row %)	145 (74.0)	29 (14.8)	22 (11.2)	196 (100)

^a There was evidence of an association between VA status and ELD visibility ($P < .0008$).

The midpoint ELD width could be measured on MR imaging in all (22/22) of the type 3 ears and in 21/29 (72.4%) of type 2 ears. The mean ELD width was 1.39 (SD, 0.78) mm for all measurable ears, 0.79 (SD, 0.16) mm for type 2 ears, and 1.96 (SD, 0.70) mm for type 3 ears. Among EVA+ ears with measurable ELDs on MR imaging (30 total), 6 (20%) had an ELD width of <1 mm, including 4 ears rated as type 2 and 2 ears rated as type 3. All 24 ears in which the ELD midpoint width was ≥ 1 mm (including 4 type 2 ears and 20 type 3 ears) were EVA+ on CT. An enlarged extraosseous ELS was visible in 21 ears, all of which were EVA+ on HRCT and type 3 on MR imaging with axial ELS dimensions ranging from 2.1×1.6 mm to 14.1×5.5 mm.

An association was observed between the presence of EVA on HRCT and the type of MR imaging visibility ($P = .0008$). The predicted probabilities of an ear being EVA+ based on the type of ELD visibility on MR imaging was 0.053 (95% CI, 0.024–0.114) for type 1 ears, 0.288 (95% CI, 0.141–0.498) for type 2 ears, and 0.997 (95% CI, 0.194–0.999) for type 3 ears (Table 4). There was also evidence of a higher probability of EVA with a 1.5T field strength compared with a 3T field strength ($P = .031$).

There was evidence that the predicted mean VA widths differed significantly on the basis of MR imaging visibility ($P < .0001$), regardless of the location (midpoint or opercular) or the reconstruction plane (axial or Pöschl) used for VA measurement on HRCT (Table 5). Predicted mean axial midpoint VA width was 0.62 (95% CI, 0.55–0.69) mm for type 1 ears, 0.97 (95% CI, 0.83–1.11) mm for type 2 ears, and 2.08 (95% CI, 1.92–2.25) mm for type 3 ears. There was evidence that all the predicted mean midpoint VA widths differed significantly from each other between the different types of ELD visibility on MR imaging (Tukey-adjusted P value $< .0001$ for all comparisons).

Table 4: Predicted probability of VA enlargement based on the type of MR Imaging visibility

Type of ELD Visualization on High-Resolution MR Imaging	Predicted Probability of EVA	95% Confidence Level
Type 1	0.053	(0.024–0.114)
Type 2	0.288	(0.141–0.498)
Type 3	0.997	(0.194–0.999)

The predicted mean axial VA opercular width was 0.92 (95% CI, 0.80–1.03) mm for type 1 ears; 1.43 (95% CI, 1.20–1.67) mm for type 2 ears; and 3.00 (95% CI, 2.73–3.28) mm for type 3 ears. There was evidence that all predicted mean opercular widths differed significantly among MR imaging visibility types (Tukey-adjusted P value = .0004 for the comparison between type 1 and type 2 ears, and $< .0001$ for all other comparisons). The predicted mean midpoint VA measurements in the Pöschl plane also differed significantly from each other across all ELD visibility types (Table 5). There was evidence that the 1.5T field strength was associated with higher mean VA widths for all 3 measurements compared with 3T field strength (P values ranging from .0003 to .0051).

The results of the independent reader assessments of ELD visibility on MR imaging are summarized in Tables 6 and 7. For distinguishing the 3 types of ELD visualization separately, there was substantial agreement among the 3 readers for the right side (Fleiss $\kappa = 0.691$, 95% CI, 0.579–0.803) and moderate agreement for the left side (Fleiss kappa = 0.531; 95% CI, 0.396–0.666).¹⁶

When type 1 and type 2 visualizations were combined into a single category resulting in a dichotomized outcome variable (type 1 or type 2 versus type 3), there was almost perfect inter-reader agreement among the 3 readers with Fleiss κ values of 0.849 (95% CI, 0.714–0.984) for the right side and 0.825 (95% CI, 0.667–0.982) for the left side.¹⁶

Pair-wise analysis of reader agreement showed almost perfect agreement between readers 1 and 3 for both 3-category and 2-category ELD assessment on both sides. Reader 2 demonstrated fair-to-substantial agreement with readers 1 and 3 (Fleiss κ ; range, 0.361–0.615) in the 3-category ELD assessment (Table 7). For the 2-category ELD assessment, reader 2 showed substantial-to-almost perfect agreement with readers 1 and 3 (Fleiss κ range, 0.754–0.822).¹⁶ Overall, reader 2 rated more ears as type 2 or type 3 compared with readers 1 and 3 (Table 6).

DISCUSSION

Our findings suggest that the high-resolution CISS sequence we commonly use at our institution for inner ear assessment performs poorly for visualizing the ELD and should not be relied on

Table 5: Predicted mean VA width based on MR imaging visibility of the ELD^a

Type of ELD Visualization on High-Resolution MR Imaging	VA Midpoint Width (Axial Plane)		VA Opercular Width (Axial Plane)		VA Midpoint Width (Pöschl Plane)	
	Predicted Mean (mm)	95% CI	Predicted Mean (mm)	95% CI	Predicted Mean (mm)	95% CI
Type 1	0.62	(0.55–0.69)	0.92	(0.80–1.03)	0.59	(0.53–0.64)
Type 2	0.97	(0.83–1.11)	1.43	(1.20–1.67)	0.83	(0.72–0.94)
Type 3	2.08	(1.92–2.25)	3.00	(2.73–3.28)	1.98	(1.85–2.11)

^a All predicted means differed significantly from each other. For comparison of predicted mean VA opercular width between type 1 and type 2 ears, Tukey-adjusted $P = .0004$. For comparison of predicted mean VA midpoint width in the Pöschl plane between type 1 and type 2 ears, $P = .0005$. For all other comparisons, $P < .0001$.

Table 6: Results of 3-outcome ELD assessment on MR imaging by the 3 readers

Type of ELD Visualization on High-Resolution MR Imaging	Reader 1 (Fellow and Senior Radiologist)		Reader 2 (Junior Radiologist)		Reader 3 (Neurotologist)	
	Right	Left	Right	Left	Right	Left
Type 1	69	76	49	47	67	73
Type 2	17	12	34	38	20	16
Type 1 or 2	86	88	83	85	87	89
Type 3	12	10	15	13	11	9

Table 7: Summary of interreader agreement analysis for ELD visibility on MR imaging

Readers	3-Category Outcome: Fleiss κ (95% CI)		2-Category Outcome: Fleiss κ (95% CI)	
	Right	Left	Right	Left
All 3 readers	0.691 (0.579–0.803)	0.531 (0.396–0.666)	0.849 (0.714–0.984)	0.825 (0.667–0.982)
Pair-wise comparisons:				
Reader 1 vs 2	0.555 (0.402–0.709)	0.361 (0.186–0.537)	0.785 (0.604–0.966)	0.754 (0.547–0.960)
Reader 1 vs 3	0.935 (0.863–1.007)	0.844 (0.724–0.963)	0.951 (0.885–1.047)	0.942 (0.828–1.055)
Reader 2 vs 3	0.615 (0.468–0.762)	0.449 (0.279–0.619)	0.822 (0.654–0.991)	0.795 (0.601–0.989)

to rule out a diagnosis of EVA in children being evaluated for hearing loss. Notably, in nearly three-quarters of our sample, the ELD could not be seen on high-resolution inner ear MR imaging. The percentage of ears in which the ELD was not visible increased to >87% when we focused on EVA– ears, with the ELD being only faintly visible in the remainder. These results are in keeping with a previous study by Sarioglu et al,¹³ who reported an overall rate of ELD nonvisualization in 79.2% of all ears and 88.5% of EVA– ears on MR imaging.

However, our results diverge from those of Sarioglu et al¹³ when focusing on patients with EVA. Unlike in their report, which found an enlarged VA on MR imaging in 92.9% of EVA cases and a nonvisible VA in the remaining 7.1%, we noted that the ELD was not visible in 22.5% and was only faintly visible in another 22.5% on MR imaging in our population of EVA+ ears.

Several previous studies have reported a high concordance between HRCT and MR imaging for diagnosing EVA; however, in most of those studies, HRCT was more sensitive.^{4,7,8,10–12} Recently, Clarke et al¹⁰ found that MR imaging had a sensitivity of 97% for identifying EVA, misdiagnosing only 1 of 38 EVA+ ears. In comparison, we noted that MR imaging did a much poorer job at identifying EVA, failing to depict the ELD in 9/40 EVA+ ears in our sample. While the reason for this discrepancy is unclear, the explanation may rest, in part, on between-study differences in specific sequences used. Our study included only CISS sequences for inner ear characterization, while Clarke et al used 3D FSE sequences (T2 FSE and T2 SPACE). Some centers prefer 3D FSE sequences for inner ear evaluation because they eliminate banding artifacts, have fewer flow artifacts, and have fewer susceptibility artifacts at air-bone interfaces.^{17,18} On the other hand, the previously mentioned study by Sarioglu et al¹³ used a balanced fast-field echo MR imaging sequence, which, like CISS, is also a balanced steady free precession sequence. Whether 3D TSE sequences or other balanced steady-state gradient-echo sequences are superior to CISS for ELD evaluation is unknown, and future head-to-head comparisons between different high-resolution sequences might be helpful in elucidating this issue.

Unlike some previous studies,^{4,6,10,13} we did not specifically compare the diagnostic sensitivities of HRCT and MR imaging for diagnosing EVA, in part because agreed-upon criteria for diagnosing EVA on MR imaging do not exist. We also did not attempt to correlate VA width measurement on HRCT and ELD measurement on MR imaging, because these analyses have already been performed. Despite claims from earlier studies, it has been our observation that accurate measurement of ELD width on MR imaging is frequently problematic because the ELD is usually either not visible or only faintly resolved, making it nearly impossible to reliably measure its width in most cases. In fact, a

recent study by Saeed et al¹⁹ found only moderate agreement among independent readers in the measurement of ELD mid-point width on high-resolution MR imaging. Instead, we elected to focus on a relatively simple subjective classification for evaluating the ELD, which can be easily applied in a busy clinical setting, as was evidenced by high, nearly perfect interrater agreement for distinguishing type 3 ELDs from type 1 and 2 ELDs. The assessments of the fellow and senior radiologists demonstrated almost perfect agreement with the neurotologist in ELD assessment regardless of whether a 3-category (type 1 versus type 2 versus type 3) or 2-category (type 1 or 2 versus type 3) outcome was used, while there was less robust agreement between the junior radiologist (reader 2) and the other 2 readers. Reader 2 rated more ears as type 2 or type 3 compared with readers 1 and 3, possibly due to a lack of calibration training, because the secondary readers were provided only single examples of each ELD visualization type before their MR imaging assessments. Greater training with more exposure to the different ELD types may have resulted in a higher rate of agreement with the other readers.

Despite the limitations of MR imaging for ELD visualization and for ruling out an EVA diagnosis in our sample, type 3 ELD visualization, when present, was highly predictive of the presence of EVA, with easy ELD visualization being associated with a >99% probability of an ear being EVA+. On the basis of this observation, it might be reasonable to suggest that HRCT may not be necessary for confirming EVA when a pre-existing high-resolution MR imaging demonstrates a type 3 ELD.

The significance of type 2 ELD visualization is less clear. Although type 2 visualization was seen in more EVA+ ears than EVA– ears (22.5% versus 12.8%, respectively), the predicted probability of EVA when a type 2 ELD was seen was only 0.288, meaning that most ears demonstrating faint ELD visualization on MR imaging are EVA–. Thus, while type 2 ELD visualization is relatively uncommon in EVA– ears, it is probably normal in most cases when present.

Like previous studies, our study design has the limitations inherent in retrospective analyses. We excluded >80% of the initial screened population, largely due to lack of relevant MR imaging, significantly reducing the sample size and potentially introducing selection biases to the study. At our institution, completion of MR imaging is at the clinician's discretion, and patients in this study were more likely to have SNHL than pure conductive hearing loss because those imaged for conditions such as ear disease due to chronic eustachian tube dysfunction, congenital aural atresia, and cholesteatoma would not routinely undergo MR imaging. Nevertheless, we believe that any selection bias would likely have minimal effect on our observations and conclusions due to the nature of our study aims.

This study being performed at single center and our focusing exclusively on the CISS sequence for inner ear evaluation may limit the generalizability of our findings and explain some of the discrepancies between our results and those other previous studies. Conversely, this homogeneity of our data conferred by its single-center location and inclusion of only studies that used a CISS MR imaging sequence for the IAC evaluation may also provide some benefits of improved statistical strength to our analysis, which was nearly devoid of confounding effects due to large numbers of differing MR imaging sequences and referring facilities. Finally, increasing application of 7T and higher-field-strength imaging along with continuing advancements in hardware and sequence development will likely provide improvement in resolution and scan quality and afford better MR imaging visualization of the ELD and discrimination between normal and abnormal ELDs in the future.

CONCLUSIONS

Our findings suggest that the CISS MR imaging technique commonly used for inner ear evaluation performs poorly overall at resolving the ELD and underdiagnoses EVA in a substantial proportion of cases. However, when the ELD is easily seen on CISS MR imaging, there is a >99% probability that the VA is enlarged. On the basis of these observations, we believe that HRCT should remain the first-line imaging choice for ruling out suspected EVA; however, in cases in which an initial MR imaging demonstrates type 3 ELD visibility, HRCT imaging may not be necessary to confirm the diagnosis.

Disclosure forms provided by the authors are available with the full text and PDF of this article at www.ajnr.org.

REFERENCES

- Joshi VM, Navlekar SK, Kishore GR, et al. **CT and MR imaging of the inner ear and brain in children with congenital sensorineural hearing loss.** *Radiographics* 2012;32:683–98 [CrossRef Medline](#)
- Koesling S, Rasinski C, Amaya B. **Imaging and clinical findings in large endolymphatic duct and sac syndrome.** *Eur J Radiol* 2006;57:54–62 [CrossRef Medline](#)
- Madden C, Halsted M, Benton C, et al. **Enlarged vestibular aqueduct syndrome in the pediatric population.** *Otol Neurotol* 2003;24:625–32 [CrossRef Medline](#)
- Connor SE, Dudau C, Pai I, et al. **Is CT or MRI the optimal imaging investigation for the diagnosis of large vestibular aqueduct syndrome and large endolymphatic sac anomaly?** *Eur Arch Otorhinolaryngol* 2019;276:693–702 [CrossRef Medline](#)
- Naganawa S, Koshikawa T, Iwayama E, et al. **MR imaging of the enlarged endolymphatic duct and sac syndrome by use of a 3D fast asymmetric spin-echo sequence: volume and signal-intensity measurement of the endolymphatic duct and sac and area measurement of the cochlear modiolus.** *AJNR Am J Neuroradiol* 2000;21:1664–69 [Medline](#)
- Deep NL, Hoxworth JM, Barrs DM. **What is the best imaging modality for diagnosing a large vestibular aqueduct?** *Laryngoscope* 2016;126:302–03 [CrossRef Medline](#)
- Kachniarz B, Chen JX, Gilani S, et al. **Diagnostic yield of MRI for pediatric hearing loss: a systematic review.** *Otolaryngol Head Neck Surg* 2015;152:5–22 [CrossRef Medline](#)
- Simons JP, Mandell DL, Arjmand EM. **Computed tomography and magnetic resonance imaging in pediatric unilateral and asymmetric sensorineural hearing loss.** *Arch Otolaryngol Head Neck Surg* 2006;132:186–92 [CrossRef Medline](#)
- Parry DA, Booth T, Roland PS. **Advantages of magnetic resonance imaging over computed tomography in preoperative evaluation of pediatric cochlear implant candidates.** *Otol Neurotol* 2005;26:976–82 [CrossRef Medline](#)
- Clarke RL, Isaacson B, Kutz JW, et al. **MRI evaluation of the normal and abnormal endolymphatic duct in the pediatric population: a comparison with high-resolution CT.** *AJNR Am J Neuroradiol* 2021;42:1865–69 [CrossRef Medline](#)
- Dahlen RT, Harnsberger HR, Gray SD, et al. **Overlapping thin-section fast spin-echo MR of the large vestibular aqueduct syndrome.** *AJNR Am J Neuroradiol* 1997;18:67–75 [Medline](#)
- Deep NL, Carlson ML, Weindling SM, et al. **Diagnosing large vestibular aqueduct: radiological review of high-resolution CT versus high-resolution volumetric MRI.** *Otol Neurotol* 2017;38:948–55 [CrossRef Medline](#)
- Sarioglu FC, Cetin AC, Guleryuz H, et al; Division of Pediatric Radiology, Department of Radiology, Dokuz Eylul University School of Medicine, Izmir, Turkey. **The diagnostic efficacy of MRI in the evaluation of the enlarged vestibular aqueduct in children with hearing loss.** *Turk Arch Otorhinolaryngol* 2021;58:220–26 [CrossRef](#)
- Boston M, Halsted M, Meinzen-Derr J, et al. **The large vestibular aqueduct: a new definition based on audiologic and computed tomography correlation.** *Otolaryngol Head Neck Surg* 2007;136:972–77 [CrossRef Medline](#)
- Juliano AF, Ting EY, Mingkwansook V, et al. **Vestibular aqueduct measurements in the 45 degrees oblique (Pöschl) plane.** *AJNR Am J Neuroradiol* 2016;37:1331–37 [CrossRef Medline](#)
- Landis JR, Koch GG. **The measurement of observer agreement for categorical data.** *Biometrics* 1977;33:159–74 [Medline](#)
- Byun JS, Kim HJ, Yim YJ, et al. **MR imaging of the internal auditory canal and inner ear at 3T: comparison between 3D driven equilibrium and 3D balanced fast field echo sequences.** *Korean J Radiol* 2008;9:212–18 [CrossRef Medline](#)
- Naganawa S, Koshikawa T, Fukatsu H, et al. **MR cisternography of the cerebellopontine angle: comparison of three-dimensional fast asymmetrical spin-echo and three-dimensional constructive interference in the steady-state sequences.** *AJNR Am J Neuroradiol* 2001;22:1179–85 [Medline](#)
- Saeed HS, Rajai A, Dixon R, et al. **Can MRI biomarkers for hearing loss in enlarged vestibular aqueduct be measured reproducibly?** *Br J Radiol* 2023;96:20220274 [CrossRef Medline](#)